Ab initio nonadiabatic molecular dynamics investigation on the dynamics of photogenerated spin hole current in Cu-doped MoS_2

Chuanyu Zhao,[1,2] Qijing Zheng,[2,*] Jianlan Wu,[1] and Jin Zhao[2,3,4,†]

[1]*Department of Physics, Zhejiang University, Hangzhou, Zhejiang 310027, China*

[2]*ICQD/Hefei National Laboratory for Physical Sciences at Microscale, and Key Laboratory of Strongly-Coupled Quantum Matter Physics, Chinese Academy of Sciences, and Department of Physics, University of Science and Technology of China, Hefei, Anhui 230026, China*

[3]*Department of Physics and Astronomy, University of Pittsburgh, Pittsburgh, Pennsylvania 15260, USA*

[4]*Synergetic Innovation Center of Quantum Information and Quantum Physics, University of Science and Technology of China, Hefei, Anhui 230026, China*

(Received 29 June 2017; revised manuscript received 16 September 2017; published 17 October 2017)

Fully spin-polarized hole current is theoretically proposed to be generated by photoexcitation in the impurity states of the MoS_2 monolayer with sulfur partially substituted by copper. To understand the dynamics of the photogenerated spin hole current, we perform a time-domain *ab initio* nonadiabatic molecular dynamics investigation with different initial excitation and temperature. First, the spin hole relaxes in a band-by-band manner. Therefore a longer lifetime can be achieved if the initial hole is generated at the lower edge of the impurity bands. Second, the phonon excitation is found to affect the spin hole dynamics significantly. When the temperature is decreased from 100 to 50 K, the hole relaxation across the band gap is strongly suppressed by the phonon bottleneck, which is due to the reduction of the phonon occupations. Our results show that the initial hole generation and phonon excitation are two key factors determining the dynamics of the photogenerated spin hole, which provide insights into the design of optimal spintronic devices.

DOI: 10.1103/PhysRevB.96.134308

I. INTRODUCTION

Electrons have both charge and spin as two different freedoms of motion. In the era of electronics, semiconductors have played fundamental roles in virtue of the versatile properties of the charge. Incorporating the spin degree of freedom into conventional semiconducting electronic devices has become a significant research subject in spintronics [1]. An active control and manipulation of the electron spin is expected to multiply the functions of semiconducting materials.

Using light to generate spin-polarized current in semiconductors has attracted a lot of research attention due to the high efficiency and energy conservation [2–8]. First, the optical response of the electron spin is on a time scale of femtoseconds, which is several orders of magnitude shorter than those operated by the electrical measures [2]. Second, the optically generated spin-polarized current is free of the Joule heating caused by the resistance between various ferromagnetic metal/semiconductor interfaces in the electrical spin injection, which requires especially tailored tunnels or Schottky barriers [1,8]. Typically, an effective optical orientation [1] is needed to generate spin-polarized current in semiconductors with significant spin-orbit coupling. In these cases, the circularly polarized light of a well-defined frequency is used because of the requirement of the optical selection rule for both angular momentum and energy of the relevant electron states. Besides that, if a spin-polarized electronic band can be separated in energy, spin current can also be generated using unpolarized light with specific frequency, which has been seldom reported [8].

In recent years, molybdenum disulphide (MoS_2) with layered crystal structure has attracted a lot of attention for its unique semiconducting properties, which have been demonstrated to be promising for device applications and spintronics [9,10]. Strong light-matter interaction makes MoS_2 a good candidate to be used for the photogenerated spin current. So far, several strategies to introduce magnetism into the nonmagnetic MoS_2 have been reported from both theoretical [11–13] and experimental [14–16] research. By the density functional theory (DFT) computation, we propose that the electronic structure of the Cu doped MoS_2 monolayer with a narrow direct band gap is close to the spin gapless semiconductors [17], in which the fully spin-polarized hole current can be generated by the excitation using an unpolarized light with an appropriate energy. With this stratagem, both electrical and magnetic properties can be controlled simultaneously by tuning the optical excitation.

The photogenerated spin hole will relax to the ground state within its lifetime, which determines the applications of such photogenerated spin hole current in spintronics. The DFT investigation can be used to propose the feasibility of the photogenerated spin-polarized hole current, however it is helpless to study the time-dependent (TD) dynamics of photogenerated carrier relaxation. In recent years, the nonadiabatic molecular dynamics (NAMD) approach formulated within the framework of time-dependent density functional theory (TDDFT) enables us to achieve valuable insights into the time evolution of photogenerated carriers. In this paper, we adopt an *ab initio* NAMD program implementing the fewest switches surface hopping (FSSH) algorithm [18] developed by Prezhdo's group [19,20] to simulate the dynamics of the spin-polarized hole in a Cu doped MoS_2 monolayer. This program is computationally tractable and has been utilized in several studies of the relaxation progress of photogenerated carriers in semiconducting materials [21–26]. We demonstrate that the initial hole generation and the phonon excitation are two key factors that determine the dynamics of the

*zqj@mail.ustc.edu.cn
†zhaojin@ustc.edu.cn

photogenerated hole. The lifetime for the spin-polarized hole current can be extended by generating holes using larger excitation energy, or by decreasing phonon occupation through temperature decreasing.

The organization of this paper is as follows. The details of NAMD calculations are provided in Sec. II. The simulation results and discussions are shown in Sec. III. Finally, we present our conclusions in Sec. IV.

II. COMPUTATIONAL METHODS

The *ab initio* NAMD simulations are carried out using homemade code Hefei-NAMD [27] which augments the Vienna *ab initio* simulation package (VASP) [28] with the NAMD capabilities within TDDFT similar to Refs. [19,20]. In this NAMD simulation, the static and *ab initio* molecular dynamics (AIMD) calculations are carried out using VASP [28]. The projector-augmented wave pseudopotentials [29,30] and the Perdew-Burke-Ernzerhof exchange-correlation functional [31,32] are adopted to construct the single-electron Hamiltonian. The cutoff for the plane-wave basis is 500 eV, and the width for the Gaussian smearing method is 0.05 eV. A 6 × 4 rectangular supercell of a MoS_2 monolayer is shown in Fig. 1(b), with two S atoms in the same layer substituted by two Cu atoms along the *Y* direction. A vacuum region of about 15 Å in the *Z* direction is used to build the slab model.

After the geometry optimization, we use velocity rescaling to bring the temperature of the system to either 100 or 50 K; a 3-ps microcanonical *ab initio* molecular dynamics trajectory is then generated with a time step of 1 fs. Using the molecular dynamics trajectory, the NAMD results are based on averaging

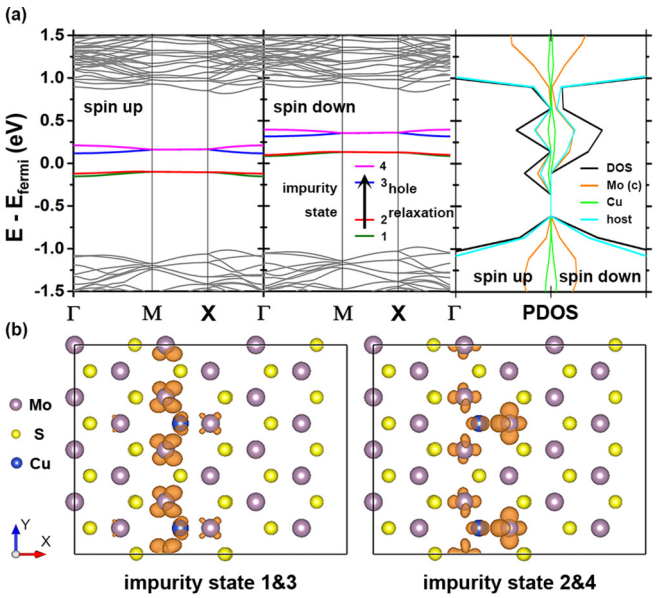

FIG. 1. The spin-polarized band structure and the projected density of states (PDOS) (a) and the orbital spatial distribution of the Cu doped MoS_2 (b). The total density of states (DOS) is projected on the coordinated Mo atoms, the Cu impurity atoms, and the rest of the MoS_2 host in the supercell. The isosurface value in (b) is set at 0.002*e* bohr. The process of spin hole relaxation within the impurity states is indicated by the arrow in Fig. 1(a).

over 100 different initial configurations. For each chosen structure, we sample 2×10^4 trajectories for the last 2 ps. We study the dynamics of the excited spin-polarized hole using NAMD as implemented within TDDFT [19,20]. In the Kohn-Sham (KS) representation [33], the TD charge density is obtained from the TD single-particle KS orbitals $\psi_p(\boldsymbol{r},t)$ as

$$\rho(\boldsymbol{r},t) = \sum_{p=1}^{N_e} |\psi_p(\boldsymbol{r},t)|^2, \tag{1}$$

where $p = 1, 2, \ldots, N_e$, and N_e is the number of electrons. Applying the TD variational principle to the KS energy generates a set of single-particle equations for the evolution of the KS orbitals:

$$i\hbar \frac{\partial \psi_p(\boldsymbol{r},t)}{\partial t} = H(\boldsymbol{r},\boldsymbol{R},t)\psi_p(\boldsymbol{r},t). \tag{2}$$

The Hamiltonian is time dependent through the change of the external potential which is produced by the motion of the atoms. For a given nuclear configuration at each moment during the evolution of the system, a set of adiabatic KS basis φ_k is obtained with DFT to expand the KS orbitals:

$$\psi_p(\boldsymbol{r},t) = \sum_k c_k(t)\varphi_k(\boldsymbol{r},\boldsymbol{R}(t)). \tag{3}$$

Inserting Eq. (3) into Eq. (2) gives the equation describing the evolution of the adiabatic basis coefficients:

$$i\hbar \frac{\partial c_j(t)}{\partial t} = \sum_k c_k(t)(\varepsilon_k \delta_{jk} + d_{jk}), \tag{4}$$

where ε_k is the energy of the adiabatic state k, and d_{jk} is the nonadiabatic coupling (NAC) between the state k and j which is given by

$$\begin{aligned} d_{jk} &= -i\hbar\langle\varphi_j|\frac{\partial}{\partial t}|\varphi_k\rangle = -i\hbar\langle\varphi_j|\nabla_{\boldsymbol{R}}|\varphi_k\rangle \dot{R} \\ \dot{R} &= -i\hbar\frac{\langle\varphi_j|\nabla_{\boldsymbol{R}}H|\varphi_k\rangle}{\varepsilon_k - \varepsilon_j}\dot{R}. \end{aligned} \tag{5}$$

The hopping of the electron or hole is determined by the NAC matrix [19,20]. From this expression, one can find that the NAC is dependent on the energy difference of the interacting states, the spatial distribution of the TD states k and j, and the nuclear velocity. All of these factors are affected by the phonon excitation and electron-phonon coupling.

During the NAMD process, the energy relaxation of the electron or hole is evaluated by computing the averaged energy:

$$\bar{\varepsilon} = \sum_k a_k \varepsilon_k, \tag{6}$$

where a_k is the population of the adiabatic state k, namely, $c_k^* c_k$. Taking the time derivative of Eq. (6) gives the expression for the adiabatic (AD) and nonadiabatic (NA) contributions to the energy relaxation:

$$\frac{d\bar{\varepsilon}}{dt} = \sum_k \left(\frac{da_k}{dt}\varepsilon_k + a_k\frac{d\varepsilon_k}{dt}\right). \tag{7}$$

The change in the averaged energy described by the first term above is due to change of the population of each adiabatic

state, namely, the hopping of the charge carrier, which is defined as the NA contribution to energy relaxation. The second term originates from change in the energy of each adiabatic state while the population is fixed, which can be attributed to the AD contribution. Using such definitions, the process of energy relaxation is divided into AD and NA parts by integrating the two terms above separately within each time interval.

To solve Eq. (4) numerically, we adopt the FSSH algorithm which provides a probability for hopping between interacting states based on the evolution of the adiabatic basis coefficients [18,20]. Furthermore, assuming that the dynamics of the valence electrons little affects the dynamics of the nuclei, the classical path approximation is made to enhance the computational efficiency by realizing the FSSH algorithm along one predetermined nuclear trajectory [20]. The hopping probability is scaled by a Boltzmann factor to ensure the detailed balance between the upward and downward transitions in energy [20].

III. RESULTS AND DISCUSSION

A. Atomic and electronic structure of the MoS_2 monolayer doped with Cu

The impurity concentration in our paper is 8.3%. The formation energy of Cu substitution depends weakly on the impurity concentration and structure. (The details are shown in the Supplemental Material [34]). Different from substituting Cu on the Mo site [35], there is only a small change in the lattice of the MoS_2 monolayer after substituting Cu on the S site [13]. The Cu impurity moves slightly outward from the doped S layer of the MoS_2 host by 0.23 Å, and the C_{3v} symmetry between the Cu impurity and three coordinated Mo atoms is maintained. As proposed in a previous theoretical research [13], the single Cu doping created by substitution of one S atom produces a magnetic moment of $1\mu_B$, which arises from one unpaired $4d$ electron distributed at the coordinated Mo atoms. When the Cu impurities in the same S layer are aligned along the Y direction as shown in Fig. 1(b), a strong ferromagnetic (FM) order can be established by superexchange between the local spin of each Cu atom. Based on the Heisenberg model with the mean-field approximation, the Curie temperature is estimated to be around room temperature, which is robust against the test of the on-site Coulomb repulsion.

Before the NAMD simulations, it is instructive to establish the electronic structure of the system. Figure 1(a) shows the spin-polarized band structure of Cu doped MoS_2. Within the energy gap of the MoS_2 monolayer, the Cu substitutions introduce four localized impurity states. A direct band gap appears at the Γ point where the spin-conserved gap between the spin-up valance-band maximum (VBM) and conduction-band minimum (CBM) is 0.24 eV, close to the spin-flip gap of 0.21 eV between the spin-up VBM and the spin-down CBM. Due to the Coulomb interaction between neighboring Cu atoms, the degeneracy of the impurity states with similar spatial orbital distribution as shown in Fig. 1(b) is lifted. The electrons on the impurity state 1 and 2 participate in the FM order establishment. Because of the FM in this Cu doped MoS_2, fully spin-polarized holes on impurity state 1 and 2 can be generated by photoexcitation [17]. In the following, we study the dynamics of such spin-polarized holes.

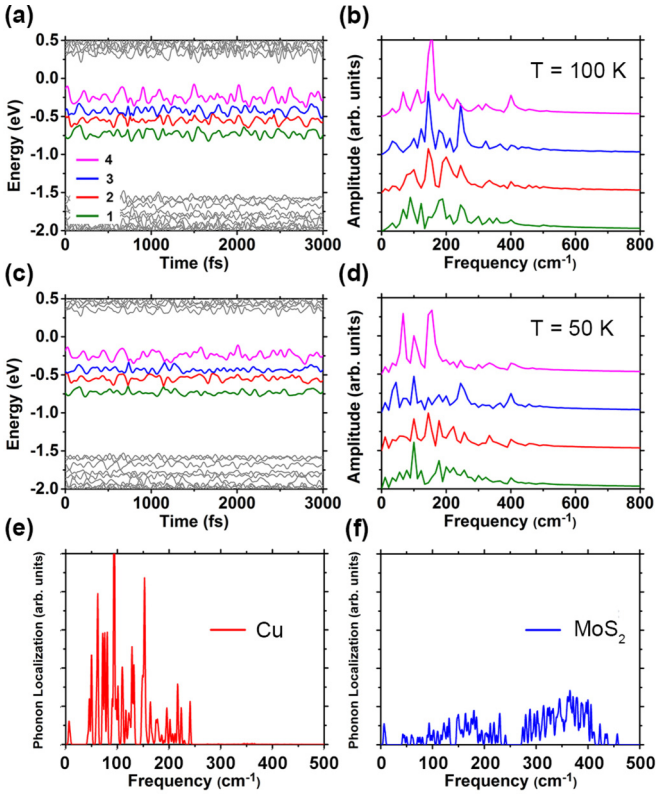

FIG. 2. Time-dependent evolution of the energy of the impurity states at the Γ point (a, c) and the FT spectra to the autocorrelation function of the energy evolution (b, d) at 100 and 50 K, respectively. The color legend is the same as shown in Fig. 1(a). (e, f) The spatial localization of each normal phonon mode projected on the Cu impurity and MoS_2 host, respectively.

B. Thermal fluctuation of the impurity states

The lifetime of the spin-polarized hole is determined by the dynamics of hole relaxation within the impurity bands as indicated by the arrow in Fig. 1(a). Once the hole relaxes across the Fermi energy, the spin-polarized hole current disappears. Therefore, we concentrate on the dynamics of the hole within the four spin-up impurity states at the Γ point as shown in Fig. 1(a). We plot the time-dependent energy evolution of these selected four impurity states with the bulk states in MoS_2 during a 3-ps AIMD trajectory at 100 K in Fig. 2(a). The energy fluctuation amplitudes of the impurity states are within 0.19–0.30 eV, much larger than that of the bulk states in MoS_2, suggesting that these impurity states have strong electron-phonon (e-p) coupling. The dominate phonon modes in e-p coupling can be seen from the Fourier transform (FT) spectra of the autocorrelation function of the energy evolution [Fig. 2(b)]. It can be seen that the impurity states are mainly coupled to the phonons within 70–240 cm^{-1}, which is the region of acoustic phonons in MoS_2 [36], indicating that these phonons are significantly scattered by the Cu impurities. This can be further understood by calculating the normal phonon modes of Cu doped MoS_2 and projecting the localization of

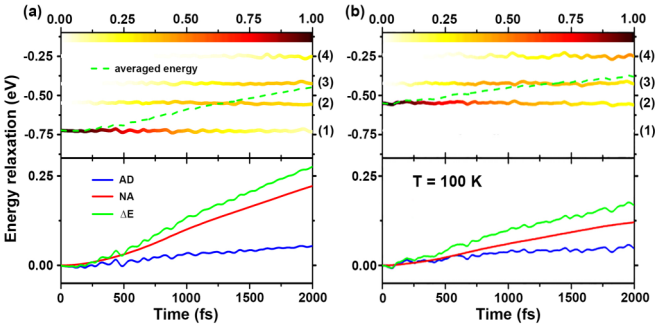

FIG. 3. The dynamics of a photogenerated hole at 100 K. The averaged energy of the hole and the population on each impurity state are shown in the upper panel, and the AD and NA contributions to the energy relaxation are shown in the lower panel with the initial state specified at the impurity state 1 (a) and 2 (b).

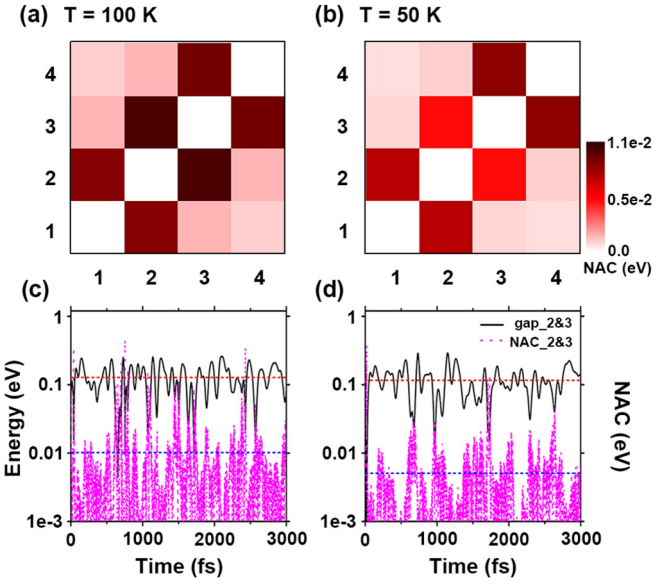

FIG. 4. The averaged absolute values of the NAC along the 3-ps trajectory between the impurity states at (a) 100 K and (b) 50 K. The absolute values of the NAC (magenta dotted line) and the oscillation of the gap (black solid line) between the impurity state 2 and 3 along the 3-ps AIMD trajectory at (c) 100 K and (d) 50 K. The blue and red dotted lines indicate the averaged value of the NAC and the gaps, respectively.

them on the Cu impurity. From Fig. 2(e) one can see that the Cu induced impurity modes distribute within 50–250 cm^{-1}, coupled strongly with the acoustic modes of MoS_2. Such impurity scatterings with bulk phonon modes within a wide range lead to the violent fluctuations of the impurity states through e-p coupling.

C. Dynamics of the photogenerated hole with different initial states

With different excitation energies, the spin-polarized hole can be generated from different initial states [state 1 or 2 in Fig. 1(a)]. At 100 K, if the hole is excited from state 1, after 2 ps, 61% of the hole has relaxed across the Fermi energy (i.e., to the impurity states 3 and 4) as shown in Fig. 3(a). In this case the lifetime is estimated to be about 3 ps. By contrast, 73% of the hole has relaxed if the hole is excited from the impurity state 2 with the lifetime estimated to be around 2.5 ps as shown in Fig. 3(b). This can be understood by checking the upper panel of Figs. 3(a) and 3(b), where the hole population decays mainly through a band-by-band process. Therefore the lifetime is longer for the spin-polarized hole excited from a deeper initial state.

We also plot the energy relaxation with the AD and NA contributions distinguished by Eq. (7) in the lower panel of Figs. 3(a) and 3(b). The energy relaxation is mainly determined by the AD mechanism within the beginning 200 fs. During this period the population decays little, therefore the energy change arises mainly from the fluctuation of the initial state. In the longer time scale, the NA mechanism makes the major contribution through hole hopping from one state to another to the band-by-band hole relaxation.

The hole hopping between different impurity states through the NA mechanism is determined by the NAC as defined in Eq. (5). In Fig. 4(a), we plot the averaged absolute values of the NAC along the 3-ps trajectory between the impurity states at 100 K. The NAC between the neighboring states is much larger than that between the separated states. Therefore the hopping to the neighboring state of the photogenerated hole is much easier than that to the separated state. This can be understood from Eq. (5) where one can see that the NAC is inversely proportional to the energy difference $\varepsilon_k - \varepsilon_j$ between electronic states k and j. The energy difference between neighboring impurity states is the smallest and therefore the NAC is the largest. Figure 4(c) shows the TD band gap, namely, the energy difference between state 2 and 3 and the NAC between them. One can also see that NAC always reaches the maximum when the band gap reaches the minimum. This explains the band-by-band character of the hole relaxation.

D. The influence of temperature on dynamics

The NAC is also strongly affected by phonon excitation and e-p coupling. From Eq. (5), except the energy difference $\varepsilon_k - \varepsilon_j$, the TD orbital coupling of state k and j $\langle\varphi_j|\nabla_{\boldsymbol{R}} H|\varphi_k\rangle$ can be understood as e-p coupling elements, and the nuclear velocity $\dot{R}$ is associated with phonon excitation. Therefore, a certain temperature dependence is expected in the dynamics process. To verify this, we perform the NAMD simulation at a lower temperature of 50 K. As shown in Figs. 2(c) and 2(d), the amplitudes of the energy fluctuations are narrowed to 0.14–0.25 eV as a result of the phonon occupation reduction. The corresponding Fourier-transform spectra are also shifted to lower frequency compared with the spectra of 100 K. The phonon occupation reduction induces the decrease of NAC. Especially, as shown in Figs. 4(b) and 4(b), the NAC between state 2 and 3 decreases significantly from 0.01 to 0.005 eV at 50 K, which suppresses hole relaxation across the band gap. The energy difference term plays a minor role here since it changes insignificantly with the temperature. (See the Supplemental Material [34] for details). The nuclear velocity and e-p coupling elements are the major factors. At 50 K state 2 and 3 couple to phonon modes with different frequencies.

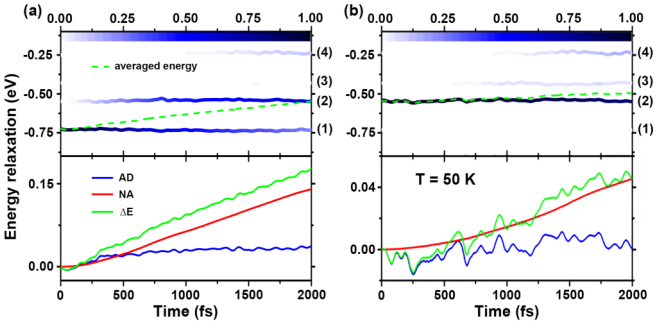

FIG. 5. The dynamics of a photogenerated hole at 50 K. The averaged energy of the hole and the population on each impurity state are shown in the upper panel, and the AD and NA contributions to the energy relaxation are shown in the lower panel with the initial state specified at the impurity state 1 (a) and 2 (b).

Yet when the temperature increases to 100 K, state 2 and 3 mostly couple to the same phonon modes. Such a coherent e-p coupling between state 2 and 3 may enhance the increasing of the NAC element along with the temperature and induce the strong temperature dependence. The NAMD results are shown in Fig. 5; the band-by-band relaxation is the same as in the case of 100 K. However, the hole relaxation proportion at 2 ps is strongly suppressed to 14 and 21% with respect to different initial states, which signifies a phonon bottleneck for the hole relaxation across the band gap. For the excitation from state 1 and 2, the lifetime of the spin-polarized hole is extended to 10 and 7.5 ps, respectively, about three times longer than that of 100 K. The suppression of photogenerated hole decay also results in a much longer period of AD determined energy relaxation for about 500 fs as shown in the lower panel of Figs. 5(a) and 5(b).

E. Discussion

In this paper, the set of adiabatic KS bases as shown in Eq. (3) is only sampled at the Γ point in the first Brillouin zone, which is proposed to give a reasonable evaluation for the lifetime of the hole current. First, the impurity states which are contributed by the 4*d* orbitals of the coordinated Mo atoms exhibit localized spatial distributions as shown in Fig. 1(b), suggesting a weak dispersion in the momentum space. Second, the system maintains the direct band gap after the Cu substitution, where the photogenerated hole relaxes at the Γ point. Third, we perform the simulations using a large 6 × 4 rectangular supercell, which has a small Brillouin zone, suggesting the investigation at the Γ point is enough.

There are also some limitations in our investigation. First, the set of adiabatic KS bases in our simulation is restricted in the spin-up subspace. The spin-flip gap is close to the spin-conserved gap as stated in Sec. III (A); the spin-down KS basis can only accelerate the intraband relaxation; therefore, we ignore the influence of spin flip on the band-by-band relaxation across the band gap. Moreover, the thermal fluctuation of the structure in the real system can cause the hole to be not fully spin polarized. Since we perform the NAMD simulation at much lower temperatures relative to the theoretically predicted Curie temperature of the system, the thermal fluctuation on the spin orientation can be ignored. In order to give a comprehensive description including the spin flip during the NAMD process, the set of adiabatic KS bases has to be expanded to include both spin subspaces. Second, we use the single-electron Hamiltonian to simulate the excited hole dynamics. Therefore the exciton effects are not included which are known to be important in two-dimensional materials [37,38]. Yet as shown in a recent study impurity doping usually increases the density of charge carrier and thus enhances the screening effects, which can reduce the exciton binding energy and make the exciton effects less significant [39]. Third, the spin-orbit coupling also has to be added to the Hamiltonian to establish an effective coupling between the different spin subspaces. However, our investigation of the band structure including the spin-orbital coupling shows spin-orbital coupling effects are insignificant. The change of the band gap is at the magnitude of meV (see the Supplemental Material [34] for more details). Therefore we believe that it will not change the lifetime of the photogenerated spin hole distinctly. Still we believe the generalization of NAMD including the exciton binding and spin-orbit coupling is an important project in the future.

Our paper shows that the photogenerated spin hole dynamics is strongly affected by the e-p coupling. Therefore lattice strain can be an important tuning factor since it can affect the electromechanical properties of the MoS_2 monolayer by significantly altering the in-plane and out-of-plane phonon modes [40]. On the other hand, strain can also dramatically change the electronic structure of the MoS_2 monolayer at zero temperature [41]. The interplay between strain and dynamics in the MoS_2 monolayer is indeed another valuable research project for the future.

IV. CONCLUSIONS

Using an *ab initio* NAMD approach, we simulate the dynamics of the spin-polarized holes in the Cu doped MoS_2 monolayer as a function of the initial state and the temperature. First, we find that the hole relaxation primarily occurs by a band-by-band process. Second, the energy relaxation is approximately linear with time during the beginning 2 ps. The nonadiabatic process of energy relaxation follows the adiabatic process, which is on the scale of hundreds of femtoseconds. Third, when the temperature is decreased from 100 to 50 K, the hole relaxation across the band gap is strongly suppressed by the phonon bottleneck, which is due to the reduction of the phonon occupations. These results suggest that the initial hole generation and the phonon excitation are two key factors that can be used to tune the dynamics of the photogenerated hole with full spin polarization in the Cu doped MoS_2 monolayer. A longer lifetime for the spin-polarized hole current can be obtained by generating holes on the lower edge of the impurity states, or by decreasing the temperature. Our results provide valuable insights into the design of materials and devices for spintronics.

ACKNOWLEDGMENTS

J.Z. acknowledges the support of the Ministry of Science and Technology of China, Grants No. 2016YFA0200604 and

No. 2017YFA0204904; National Natural Science Foundation of China, Grants No. 11620101003, No. 21373190, and No. 21421063; and the Fundamental Research Funds for the Central Universities, Grant No. WK3510000005. J.W. acknowledges the support of National Natural Science Foundation of China, Grant No. 21573195. Calculations were performed at Environmental Molecular Sciences Laboratory at the Pacific Northwest National Laboratory, a user facility sponsored by the US Department of Energy Office of Biological and Environmental Research and supercomputing center at University of Science and Technology of China.

[1] I. Žutić, J. Fabian, and S. D. Sarma, Rev. Mod. Phys. **76**, 323 (2004).
[2] P. Němec, E. Rozkotová, N. Tesařová, F. Trojánek, E. De Ranieri, K. Olejnik, J. Zemen, V. Novák, M. Cukr, P. Malý, and T. Jungwirth, Nat. Phys. **8**, 411 (2012).
[3] G. Lampel, Phys. Rev. Lett. **20**, 491 (1968).
[4] R. R. Parsons, Phys. Rev. Lett. **23**, 1152 (1969).
[5] D. T. Pierce and F. Meier, Phys. Rev. B **13**, 5484 (1976).
[6] R. C. Myers, M. H. Mikkelsen, J.-M. Tang, A. C. Gossard, M. E. Flatté, and D. D. Awschalom, Nature Mater. **7**, 203 (2008).
[7] X. Chen, T. Yan, B. Zhu, S. Yang, and X. Cui, ACS Nano **11**, 1581 (2017).
[8] B. Endres, M. Ciorga, M. Schmid, M. Utz, D. Bougeard, D. Weiss, G. Bayreuther, and C. H. Back, Nat. Commun. **4**, 2068 (2013).
[9] B. Radisavljevic, A. Radenovic, J. Brivio, V. Giacometti, and A. Kis, Nature Nanotech. **6**, 147 (2011).
[10] S. Z. Butler, S. M. Hollen, L. Cao, Y. Cui, J. A. Gupta, H. R. Gutiérrez, T. F. Heinz, S. S. Hong, J. Huang, A. F. Ismach, E. Johnston-Halperin, M. Kuno, V. V. Plashnitsa, R. D. Robinson, R. S. Ruoff, S. Salahuddin, J. Shan, L. Shi, M. G. Spencer, M. Terrones, W. Windl, and J. E. Goldberger, ACS Nano **7**, 2898 (2013).
[11] A. Ramasubramaniam and D. Naveh, Phys. Rev. B **87**, 195201 (2013).
[12] Q. Chen, Y. X. Ouyang, S. J. Yuan, R. Z. Li, and J. L. Wang, ACS Appl. Mater. Interfaces **6**, 16835 (2014).
[13] C. Zhao, C. Jin, J. Wu and W. Ji, J. Appl. Phys. **120**, 144305 (2016).
[14] L. Cai, J. He, Q. Liu, T. Yao, L. Chen, W. Yan, F. Hu, Y. Jiang, Y. Zhao, T. Hu, Z. Sun, and S. Wei, J. Am. Chem. Soc. **137**, 2622 (2015).
[15] J. Zhang, J. M. Soon, K. P. Loh, J. Yin, J. Ding, M. B. Sullivian, and P. Wu, Nano Lett. **7**, 2370 (2007).
[16] H. P. Komsa, J. Kotakoski, S. Kurasch, O. Lehtinen, U. Kaiser, and A. V. Krasheninnikov, Phys. Rev. Lett. **109**, 035503 (2012).
[17] X. L. Wang, Phys. Rev. Lett. **100**, 156404 (2008).
[18] J. C. Tully, J. Chem. Phys. **93**, 1061 (1990).
[19] C. F. Craig, W. R. Duncan, and O. V. Prezhdo, Phys. Rev. Lett. **95**, 163001 (2005).
[20] A. V. Akimov and O. V. Prezhdo, J. Chem. Theory Comput. **9**, 4959 (2013).
[21] K. G. Reeves, A. Schleife, A. A. Correa, and Y. Kanai, Nano Lett. **15**, 6429 (2015).
[22] S. Kilina, K. A. Velizhanin, S. Ivanov, O. V. Prezhdo, and S. Tretiak, ACS Nano **6**, 6515 (2012).
[23] S. V. Kilina, D. S. Kilin, and O. V. Prezhdo, ACS Nano **3**, 93 (2009).
[24] R. Long and O. V. Prezhdo, Nano Lett. **16**, 1996 (2016).
[25] Z. Nie, R. Long, L. Sun, C.-C. Huang, J. Zhang, Q. Xiang, D. W. Hewak, Z. Shen, O. V. Prezhdo, and Z.-H. Loh, ACS Nano **8**, 10931 (2014).
[26] W. Chu, W. A. Saidi, Q. Zheng, Y. Xie, Z. Lan, O. V. Prezhdo, H. Petek, and J. Zhao, J. Am. Chem. Soc. **138**, 13740 (2016).
[27] http://staff.ustc.edu.cn/∼zhaojin/code.html.
[28] G. Kresse and J. Furthmüller, Phys. Rev. B **54**, 11169 (1996).
[29] P. E. Blöchl, Phys. Rev. B **50**, 17953 (1994).
[30] G. Kresse and D. Joubert, Phys. Rev. B **59**, 1758 (1999).
[31] J. P. Perdew, K. Burke, and M. Ernzerhof, Phys. Rev. Lett. **77**, 3865 (1996).
[32] J. P. Perdew, J. A. Chevary, S. H. Vosko, K. A. Jackson, M. R. Pederson, D. J. Singh, and C. Fiolhais, Phys. Rev. B **46**, 6671 (1992).
[33] E. Runge and E. K. U. Gross, Phys. Rev. Lett. **52**, 997 (1984).
[34] See Supplemental Material at http://link.aps.org/supplemental/10.1103/PhysRevB.96.134308 for the computational details.
[35] X. Fan, Y. An, and W. Guo, Nanoscale Res. Lett. **11**, 154 (2016).
[36] A. Molina-Sanchez and L. Wirtz, Phys. Rev. B **84**, 155413 (2011).
[37] C. Mai, A. Barrette, Y. Yu, Y. G. Semenov, K. W. Kim, L. Cao, and K. Gundogdu, Nano Lett. **14**, 202 (2014).
[38] A. Singh, G. Moody, S. Wu, Y. Wu, N. J. Ghimire, J. Yan, D. G. Mandrus, X. Xu, and X. Li, Phys. Rev. Lett. **112**, 216804 (2014).
[39] S. Gao, Y. Liang, C. D. Spataru, and L. Yang, Nano Lett. **16**, 5568 (2016).
[40] M. Ghorbani-Asl, N. Zibouche, M. Wahiduzzaman, A. F. Oliveira, A. Kuc, and T. Heine, Sci. Rep. **3**, 2961 (2013).
[41] K. He, C. Poole, K. F. Mak, and J. Shan, Nano Lett. **13**, 2931 (2013).